Water Practice & Technology

IWA PUBLISHING

Water Practice & Technology Vol 18 No 7, 1711 doi: 10.2166/wpt.2023.101

Preparation of leonardite powder-embedded calcium alginate beads and adsorption of Safranin-O dye

Nihan Canan Ozdemir[a], Mohammed Saleh [b,*], Zeynep Bilici[a], Hudaverdi Arslan[a] and Nadir Dizge[a]

[a] Department of Environmental Engineering, Mersin University, Mersin 33343, Turkey
[b] National Agricultural Research Centre (NARC), Jenin, Palestine
*Corresponding author. E-mail: muh.saleh89@gmail.com

MS, 0000-0002-3145-4457

ABSTRACT

In this study, calcium alginate (Ca-Alg) beads were mixed with leonardite powder to prepare leonardite-embedded calcium alginate (Leo-Ca-Alg) beads. The prepared Leo-Ca-Alg beads were utilized for the adsorption of the Safranin-O dye. Leo-Ca-Alg beads were characterized by X-ray diffraction, Fourier transform infrared, and scanning electron microscopy before and after the adsorption process. The effects of pH, adsorbent dose, initial dye concentration, and contact time on the adsorption of Safranin-O dye onto Leo-Ca-Alg beads were investigated. The optimal condition was achieved at a pH value of 8.0, an adsorbent amount of 20 g/L, an initial concentration of 10 mg/L, and a contact time of 120 min. Under optimum conditions, 98.91% dye removal efficiency was obtained. Besides, the isotherm, kinetic, and thermodynamic were studied for the adsorption process. Accordingly, the removal of Safranin-O dye by the Leo-Ca-Alg adsorbent can be defined by the Freundlich model and described by the Elovich model and the second-order kinetic model at concentrations of 10 and 20–30 mg/L, respectively. The Safranin-O removal by Leo-Ca-Alg was feasible and naturally spontaneous. In reuse cycle studies, it was tried up to 10 reuses and decreased from 98.91 to 83.01% in the 10th use.

Key words: adsorption, calcium alginate beads, leonardite powder, Safranin-O dye

HIGHLIGHTS

- A novel leonardite-embedded calcium alginate beads adsorbent was prepared.
- Safranin-O was removed using the prepared adsorbent with an efficiency of 98.91%.
- The Safranin-O removal by leonardite-embedded calcium alginate was feasible and naturally spontaneous.
- The adsorbent was successfully utilized for 10 cycles.

GRAPHICAL ABSTRACT

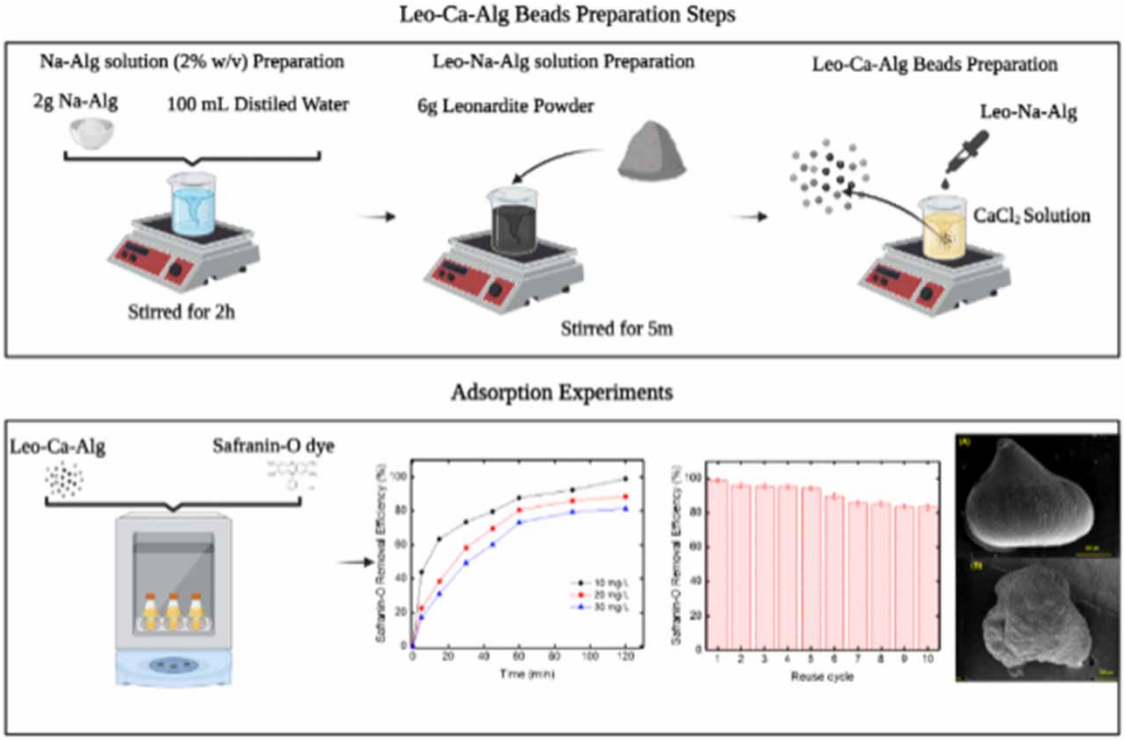

1. INTRODUCTION

Water pollution has become one of the most critical issues due to the unprecedented growth in industrialization (Mashkoor & Nasar 2020a), which discharges several pollutant types into the water bodies without any treatment (Abd-alla & Aly 1991; Mashkoor & Nasar 2020b). Dyes pollution is one of the most common types, which affects water quality even if it is found in trace concentrations (Anbia *et al.* 2010; Chanpiwat *et al.* 2015). Dyes have several properties such as high solubility in water, seldom biodegradable, and toxicity, which make the polluted water to disturb human health, aquatic living organisms, and the visual appearance of water (Kenawy *et al.* 2022). Barizão *et al.* (2020) stated that the effects of the dye on humans range from skin diseases to cancer (de Lima Barizão *et al.* 2020). All over the world, 7,105 tons were annually produced, and 2% of these amounts were discharged into the environment by different industrial sectors (Ip *et al.* 2009). The leading industries in dye consumption and discharging are textile, nutrition, leather tanning, paper, paints, light-harvesting solar cells, and photo electrochemical cells (Roy & Saha 2021). The cationic Safranin-O dye is one of the most widely used (Bensalah *et al.* 2021).

Safranin-O dye has a rubicund brown colour and enters distinct industries such as food colouring, cotton colouring, fibres, homespun, silk, flashing, and sheet (Ahmad *et al.* 2015, 2016; Adegoke *et al.* 2017; Ojo *et al.* 2019; Pham *et al.* 2019). Hence, Safranin-O removal from industrial effluents is of prime interest. The treatment of dye wastewater is an urgent issue to protect the environment and humans. Thus, many researchers examined the chemicals, physical, and biological methods in dye-contaminated wastewater treatment (Ngoc *et al.* 2022). For example, coagulation, sedimentation, adsorption, oxidative degradation (Liu *et al.* 2021), flotation, photocatalysis, electrochemical treatment, and membrane filtration methods were employed to achieve this goal (Somsesta *et al.* 2020). Adsorption has been favoured because of its simplicity and high efficiency (Duman *et al.* 2020). Other reasons like low cost, approximately no sludge generation, and speed gave the adsorption unique advantages (Crini 2006; Burakov *et al.* 2018; Adel *et al.* 2021).

Even though the application of cost-effective treatment methods for wastewater is an urgent issue, the adsorbent material selection is just as important. In this study, calcium alginate bead was selected as an absorbent material because of its availability, affordability, biodegradability, and hydrophilicity (Fiol *et al.* 2005; Gok & Aytas 2009; Li *et al.* 2013). Besides, alginate is acknowledged as a non-hazardous matter that vehemently tolerates a natural polymer (Bedade *et al.* 2019). The linear polysaccharide family that contained 1, 4-linked

β-d-mannuronic (M) with R-l-glucuronic (G) acid residues with a random arrangement along the chain is called alginic acid or alginate. The solubility of alginate depends on the ion's valent. Accordingly, alginates are soluble with monovalent ions (alkali metals and ammonium), but insoluble with divalent or polyvalent metal ions (except Mg^{2+}) (Fourest & Volesky 1996). Alginates can form cross-linked gel beads as the monovalent/multivalent ions exchange occurs (Yang *et al.* 2016). The most common cross-linking ion is calcium (Li *et al.* 2013). Alginate exchanges the sodium with calcium to form a net of cross-linked chains with an egg box shape. The interaction between calcium and two carboxyl groups provides thermal resistance and cracking prevention properties (Hu *et al.* 2017). Calcium alginate beads were used to remove different pollutants with high treatment efficiencies. Araujo *et al.* (2020) utilized calcium alginate beads and *Saccharomyces cerevisiae* for biosorption of 241Am. In another research, the removal of U(VI) by an amidoximated-modified calcium alginate gel bead with entrapped functionalized SiO nanoparticles was achieved (Khajavi *et al.* 2021). Other pollutants such as acetaminophen (de Araújo *et al.* 2022), difenoconazole and nitenpyram (Zhou *et al.* 2022), azo dye and hexavalent chromium (Bilici *et al.* 2019), Cu(II), Pb(II), Mg(II), and Fe(II) (Abou-Zeid *et al.* 2021) were also removed by alginate beads.

Leonardite is a natural low coal matter that is formed around lignite mines and has a similar structure to lignite (Ozuzun & Uzal 2021). Leonardite has higher oxygen content than lignite because leonardite contains large quantities of carboxyl and phenolic groups in its matrix (Ricca *et al.* 1993). Both materials have humic/fulvic materials making them suitable as shear thinning additives, obliging significantly in clay particles' swelling control, viscosity lowering, and filtration management (Apostolidou *et al.* 2022). Humic-based materials were employed previously as natural adsorbents for heavy metal removal (Mohan & Chander 2006; Chammui *et al.* 2014; Meng *et al.* 2017). Leonardite shows promising potential to be used as an inexpensive adsorbent as it is a naturally abundant material (Meng *et al.* 2021). According to previous studies, the functional groups and the carboxyl properties increase the adsorption capacity (Shi *et al.* 2018). A novel green adsorbent was prepared by leonardite-embedded calcium alginate (Leo-Ca-Alg) beads. The removal of Safranin-O by the prepared Leo-Ca-Alg was assessed, optimized, and the reusability was investigated.

2. MATERIALS AND METHODS

2.1. Chemicals

The source of leonardite was the district of Kahramanmaraş, Turkey. All the chemicals were acquired from Sigma-Aldrich. For bead preparation, sodium alginate (Alg) and calcium chloride dehydrate ($CaCl_2{\cdot}2H_2O$) were used. Safranin-O powder was dissolved in distilled water (1 g for 1 L) to make an adsorbate stock solution. The properties of Safranin-O are presented in Table 1. The pH values of solutions were changed by employing sodium hydroxide (NaOH, 0.1 M) and hydrochloric acid (HCl, 0.1 M).

Table 1 | Safranin-O dye common characteristics

Dye name	Chemical structure	M.W (g/mole) and formula	CAS number	pK_a	Max. wavelength λ_{max} (nm)
Safranin-O	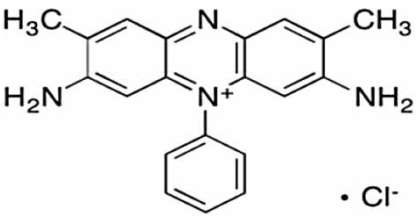	350.85 $C_{20}H_{19}ClN_4$	477-73-6	11.0	520

2.2. Preparation of Leo-Ca-Alg

To prepare the Na-Alg solution (2% w/v), 2 g of Na-Alg powder was dissolved in 100 mL deionized water and stirred for 2 h. Subsequently, 6 g leonardite (based on preliminary experiments) was mixed into the prepared solution until a homogeneous consistency was achieved (approximately 5 min). Then, the prepared Leo-Na-Alg solution was added dropwise into the $CaCl_2$ solution via a dropper to produce Leo-Ca-Alg beads. The obtained Leo-Ca-Alg beads were kept in the solution overnight and dried in an oven at 60 °C for 1 h.

2.3. Adsorption experiments

The prepared Leo-Ca-Alg beads were employed in Safranin-O dye removal via the adsorption process. The experiments were optimized for the following terms: pH, dose, time, and concentration. In the pH optimization, 20 g/L Leo-Ca-Alg beads were added to flasks with 10 mg/L dye concentration and 100 mL sample volume at different pH values (2, 4, 6, 8, and 10) and agitated for 2 h at 180 rpm. The dose optimization followed the pH experiments. Different doses of Leo-Ca-Alg (10, 20, 30, 40, and 50 g/L) were used where the appropriate amount was utilized in the kinetic study. For all experiments, the changes in the dye concentration were tracked using a UV-Visible spectrophotometer (Hach-DR 3900) at a wavelength of 520 nm, and the adsorption efficiencies were calculated by Equation (1).

$$\text{Adsorption efficiency (\%)} = \frac{C_i - C_f}{C_i} 100\% \tag{1}$$

where C_i and C_f are Safranin-O concentration at the beginning and at the end of the experiments, respectively.

The adsorption capacity (q_e, mg/g) for the prepared Leo-Ca-Alg beads was calculated according to Equation (2).

$$q_e = \frac{(C_i - C_e)}{m} V \tag{2}$$

where C_i and C_e are the Safranin-O concentrations at the beginning and the equilibrium (mg/L), respectively, m is the Leo-Ca-Alg amount (g), and V is the solution volume (L).

2.4. Kinetic experiments

The kinetic study was started by adding Leo-Ca-Alg beads to Safranin-O solutions with various concentrations (10, 20, and 30 mg/L). At variable times (0, 5, 15, 30, 45, 60, 90, and 120 min), samples were taken, and dye concentration was found. All the kinetic experiments were carried out at 180 rpm at room temperature. The adsorption capacity at any time versus the time was plotted. The adsorption mechanism was explored via different kinetic models. The pseudo-first-order model, the pseudo-second-order model, Elovich model (Elovich & Larinov 1962), intra-particle diffusion model (IDM) (López-Luna *et al.* 2019; Mallakpour & Tabesh 2019; ElHussein *et al.* 2020), and Bangham model were utilized to study the adsorption mechanism (Arslan *et al.* 2022) as shown in Equations (3)–(7), respectively.

$$q_t = q_e(1 - e^{-K_1 t}) \tag{3}$$

$$q_t = \frac{K_2 q_e^2 t}{1 + K_2 q_e t} \tag{4}$$

$$q_t = \frac{1}{b} \ln(1 + abt) \tag{5}$$

$$q_t = K_{\text{IDM}} t^{1/2} + c \tag{6}$$

$$\log\left[\log\left(\frac{C_o}{C_o - q_t m}\right)\right] = \log\left(\frac{K_b m}{2.303 V}\right) + \alpha \log(t) \tag{7}$$

where q_t is the solid-phase concentration at any time t (mg/g). K_1 is the rate constant of the pseudo-first-order kinetic model, K_2 is the reaction rate constant for the pseudo-second-order, a is the initial sorption rate (mg/g ·min), b is the desorption constant (g/mg), K_{IDM} is the IDM rate constant (mg/g·min$^{1/2}$), c is the thickness of the boundary layer, and K_b (mL/g/L) and α (<1) are Bangham's model constants.

2.5. Isotherms

The adsorptions of Safranin-O dye onto Le-Ca-Alg experiments were accomplished at distinct concentrations. As a result of these experiments, plots between the concentration and the adsorption capacity were drawn and then used to determine Langmuir (Equation (8)) and Freundlich (Equation (5)) isotherm parameters to understand the adsorbent adsorbate interaction (Equation (9)) (Yaneva *et al.* 2012; ElHussein *et al.* 2020; Hanif *et al.* 2020;

Arslan *et al.* 2022).

$$Q_e = \frac{Q_m K_L C_e}{1 + K_L C_e} \tag{8}$$

$$Q_e = K_F C_e^{1/n} \tag{9}$$

where K_L (L/mg) and K_f ((mg/g) (L/mg)$^{1/n}$) are the isotherm constants for Langmuir and Freundlich, respectively, Q_m is the maximum solid-phase concentration (mg/g), and $1/n$ is the affinity of adsorption (unitless).

2.6. Thermodynamic study

Thermodynamic studies were conducted to determine the feasibility of Safranin-O adsorption onto the prepared Leo-Ca-Alg. The study was carried out at different temperatures (25, 30, and 35 °C) for 2 h. Subsequently, the collected samples were analysed with the aid of a spectrophotometer. At the completion of experiments, the thermodynamic parameters are determined by Equations (10)–(12).

$$\Delta G = -RT\ln K_{\text{eq}} \tag{10}$$

$$\Delta G^0 = \Delta H^0 - T\Delta S^0 \tag{11}$$

$$\ln K_L = -\frac{\Delta H}{RT} + \frac{\Delta S}{R} \tag{12}$$

where ΔG, ΔH^0, and ΔS^0 are the changes in Gibbs free energy, enthalpy (J/mole), and entropy (J/K·mole), respectively. R and T are the universal gas constants (8.314 J/K·mole) and the temperature in Kelvin (K), respectively. K_{eq} is the constant of the equilibrium.

2.7. Adsorbent characterization

The prepared Leo-Ca-Alg beads were characterized to study the adsorption effects. In addition, pure Ca-Alg beads were characterized to see the difference between leonardite beads. The Leo-Ca-Alg beads were dried for 30 h at a temperature of 60 °C before the characterization step. The changes in the morphologies of Leo-Ca-Alg beads and Ca-Alg beads were identified via scanning electron microscopy (SEM; FEI, Quanta 650 Field Emission). The chemicals present at the Leo-Ca-Alg surface were scanned using energy-dispersive X-ray spectroscopy. The functional groups present at the adsorbent surface were scanned using Fourier transform infrared spectroscopy (FTIR; FT/IR-6700, Jasco) for the bands 450–4,000 cm^{-1}. X-ray diffraction (XRD; Panalytical Empyrean) was performed to determine the phases of the beads.

3. RESULTS AND DISCUSSION

3.1. Characterization of bare and Leo-Ca-Alg beads

The surface morphology is one of the most important considerations in distinguishing between bare and Leo-Ca-Alg beads. As shown in Figure 1(a), it was observed that there were differences between the bare and Leo-Ca-Alg beads. The bare bead surface showed a cracked and spherical appearance. The surface of Leo-Ca-Alg beads (Figure 1(b)) was observed to be covered with indented spherical particles. Compared to the bare bead, the surface of Leo-Ca-Alg beads showed an irregular and curved appearance.

The XRD was implemented to define the phases of the beads, as shown in Figure 2. For the raw beads (Ca-Alg), the dominant compound was calcium oxide with a cubic crystal system and Fm-3m Space group: The Lattice parameters were $a = b = c = 4.444$ A°. For the prepared Leo-Ca-Alg beads, cristobalite beta, carbon, and hematite were presented. The cristobalite beta (SiO_2) had a cubic crystal system with a space group of P 21 3 and lattice parameters of $a = b = c = 7.13$ A°. The crystal system of the carbon (C) was hexagonal and the space group of P 63/m m c. The lattice parameters were $a = 2.469$ A°, $b = 2.469$ A°, and $c = 8.841$ A°. For hematite (Fe_2O_3), the crystal system and the space group were hexagonal and R-3 c, respectively. The lattice parameters were $a = 4.918$ A°, $b = 4.918$ A°, and $c = 13.198$ A°. The XRD was also determined for the prepared Leo-Ca-Alg beads after the adsorption. Accordingly, the carbon remained as before the adsorption. But cristobalite alpha low, sodium carbide (2/2) – Ht, iron sulphate – beta, and magnetite were noticed. The crystal system of cristobalite alpha low (SiO_2) was tetragonal with the space group of P 41 21 2 (lattice parameter: $a = 4.984$ A°, $b =$

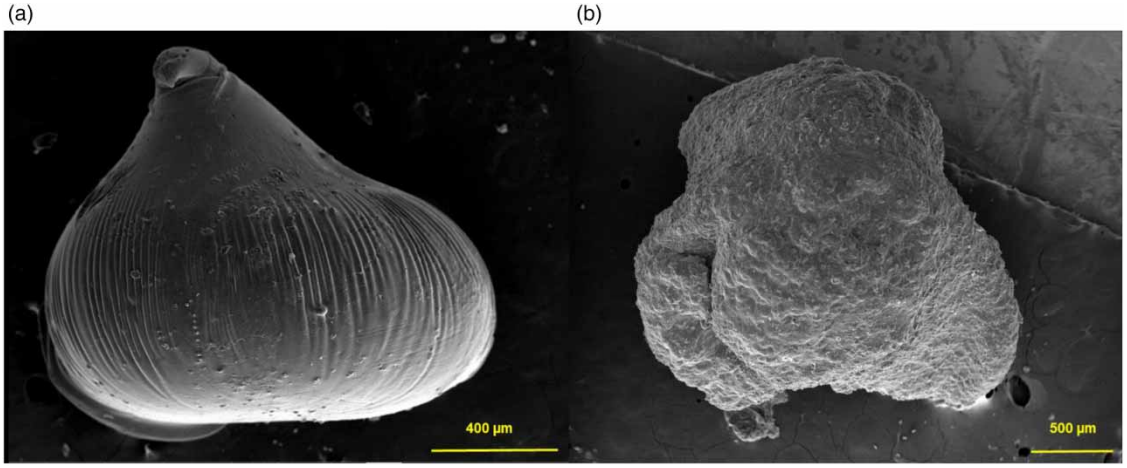

Figure 1 | SEM images for the inner surface of (a) bare and (b) Leo-Ca-Alg beads.

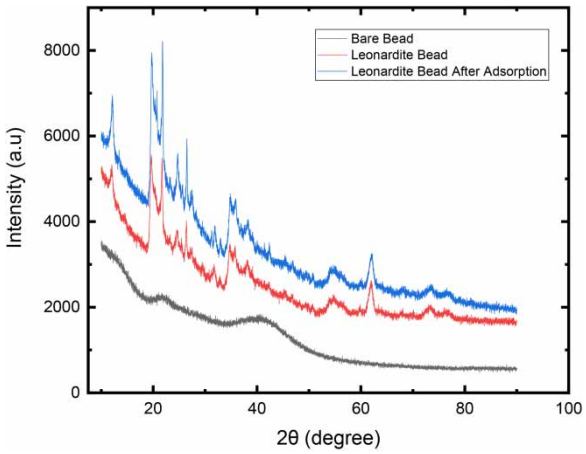

Figure 2 | XRD analysis of bare and Leo-Ca-Alg beads.

4.984 A°, and $c = 6.967$ A°). Sodium carbide (2/2) – Ht (C_2Na_2) and magnetite (Fe_3O_4) had the cubic crystal system with F m-3m and F d-3m, respectively. Sodium carbide had lattice parameters of $a = b = c = 6.7560$ A°, while magnetite had $a = b = c = 8.4810$ A°. Iron sulphate – beta (FeO_4S) with a crystal system of orthorhombic (space group: P n m a) was also recorded. The lattice parameters for the iron sulphate – beta were $a =$ 8.7150 A°, $b = 6.8040$ A°, and $c = 4.7950$ A°.

The functional groups in the raw Ca-Alg, raw Leo-Ca-Alg, and Leo-Ca-Alg beads after the adsorption process were identified using the FTIR analysis, as shown in Figure 3. Accordingly, there are more than five peaks in all spectrums, revealing that the materials are not simple. For the raw Ca-Alg beads (Figure 3(a)), there were no broad peaks in the bands 3,250–3,600 cm^{-1}, but the sharp medium peak near 3,670 cm^{-1} indicated the presence of the O-H stretching functional group. The narrow peaks just below 3,000 cm^{-1} returned to the C-C bond. No precise peak for aldehyde between 2,700 and 2,800 cm^{-1} was noticed. A triple bond functional group was noticed between the bands 2,320–2,360 cm^{-1}. The band peak observed 1,397 cm^{-1} was attributed to symmetric stretching vibrations of the COO- group. The functional group C-O stretching appeared around 1,050 cm^{-1}. Bilici *et al.* (2019) detected the O-H bond in the alginate beads for the range of 3,200–3,400 cm^{-1} and symmetric stretching vibration of COO- group at band 1,424 cm^{-1}. For the raw Leo-Ca-Alg beads (Figure 3(b)), the spectrum was changed obviously. In this context, sharp peaks near 3,620 cm^{-1} and a broad peak at 3,381 cm^{-1} were recorded. These peaks informed the presence of a hydrogen bond in the material (O-H stretching). Arslan *et al.* (2022) noticed two sharp peaks at wavelengths of 3,695 and 3,623 cm^{-1}, which referred to the presence of O-H stretching group at the leonardite powder surface. The bond at 2,987 cm^{-1} was for the C-H stretching functional group. The presence

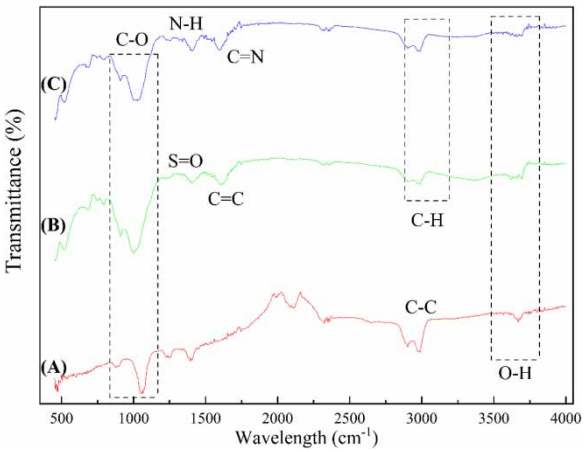

Figure 3 | FTIR analysis for (a) Ca-Alg beads, (b) raw Leo-Ca-Alg beads, and (c) Leo-Ca-Alg beads at the adsorption process end.

of the C = C group was recorded at a wavelength of 1,608 cm^{-1}. The S = O stretching was detected at 1,408 cm^{-1}. Also, the functional group C-O stretching appeared near the band 1,000 cm^{-1}. After the adsorption of Safranin-O dye, the spectrum lost its smooth shape. Besides, several peaks were noted. The most significant bond was near 1,593 cm^{-1} reflecting the presence of N-H bending group. Also, the recorded peaks between 1,650 and 1,690 cm^{-1} were related to the C = N stretching group. The appeared peaks are in consistence with the spectrum of Safranin-O dye presented previously by Sahu *et al.* (2015). The FTIR results proved that the spectrums were changed twice: the first when the Cal-Alg was modified to Leo-Ca-Alg beads and the second when the adsorption process was accomplished.

3.2. The effect of pH on adsorption of Safranin-O dye using Leo-Ca-Alg beads

The effects of solution pH on the Safranin-O adsorption onto the Leo-Ca-Alg were investigated. The removal efficiencies at a pH of 2–10 are presented in Figure 4. In general, the removal efficiency had improved proportionally with the pH values. The uptake efficiency increased sharply from 19.27% at a pH of 2 to 92.76% at a pH of 4. The further rises in the pH improved the effectiveness but in a smoother trend. The removal efficiencies at pH values 6, 8, and 10 were 94.11, 98.91, and 99.55, respectively. Previously, a significant improvement in Safranin-O dye adsorption was recorded after a pH value of 5.5 (Bensalah *et al.* 2021). The dye removal efficiencies from wastewater were determined as 98.91 and 99.55% at pH 8 and 10, respectively. However, 94.12% removal efficiency was obtained at the original pH (6) value of the wastewater. Therefore, pH 8 was chosen as the optimum pH value to prevent extra chemical consumption. The adsorption capacity had a similar pattern; the adsorption

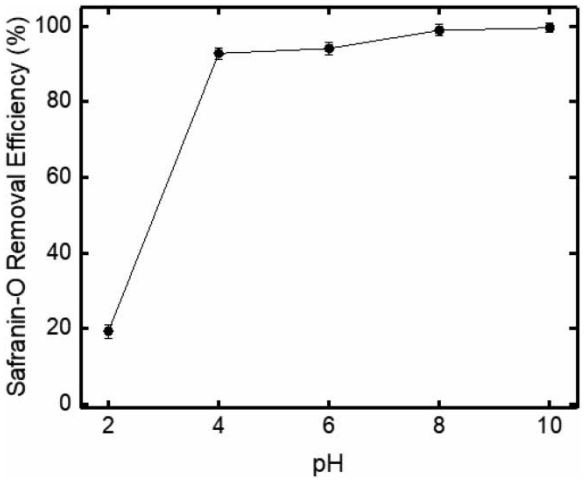

Figure 4 | The effect of pH on Safranin-O uptake using Leo-Ca-Alg beads (investigational circumstances: Leo-Ca-Alg: 20 g/L; initial Safranin-O concentration: 10 mg/L; duration: 2 h; volume: 100 mL).

capacity improved from 0.11 to 0.55 mg/g when the solution pH increased from 2 to 8. Similar results were obtained previously (Subba Reddy *et al.* 2018). The pH optimization results can be explained by the electrostatic force between Safranin-O and the Leo-Ca-Alg. Arslan *et al.* (2022) found that the surface charge of the leonardite powder goes on the negative side with the pH increases. As the negative charges increase, the potential of cationic Safranin-O dye attachment also improves. Maurya & Mittal (2013) mentioned that the deprotonation of different functional groups at the adsorbent surface increased the net electro-negativity. Thus, the removal efficiency increased. In previous studies, a reduction in the adsorption efficiency was noticed when the pH of solutions increased above 11 (Gupta *et al.* 2000; Maurya & Mittal 2013). The explanation of this phenomenon was referred to the pK_a for the Safranin-O dye. According to Harris *et al.* (2001), the pKa for safranin-O dye was 11. In this study, the reduction trend was not noticed as the maximum pH was 10.

3.3. Effect of Leo-Ca-Alg beads dose on adsorption of Safranin-O dye

The optimization experiments for the adsorbent dose were also performed. Different amounts of Leo-Ca-Alg (10, 20, 30, 40, and 50 g/L) were tested. The experiments were done in a 100 mL sample volume and a concentration of 10 mg/L at pH 8. Increasing the adsorbent dose up to 20 g/L had positively affected the dye removal efficiency (Figure 5). Beyond this dose, the adsorption efficiency did not change. The removal efficiency was 98.91% at a dosage of 20 g/L. Ghosh *et al.* (2021) stated that the high adsorbent dose improves the safranin-O removal efficiency (Ghosh *et al.* 2021). The increases in the removal efficiency were referred to the abundance of the unfilled spots at the adsorbent surface (Saleh *et al.* 2021). In contrast, the adsorption capacity had a reverse relationship with the adsorbent doses. Isik *et al.* noticed the decrease in ammonia ions and phosphate adsorption capacities when the amount of Alg beads increased (Isik *et al.* 2021b).

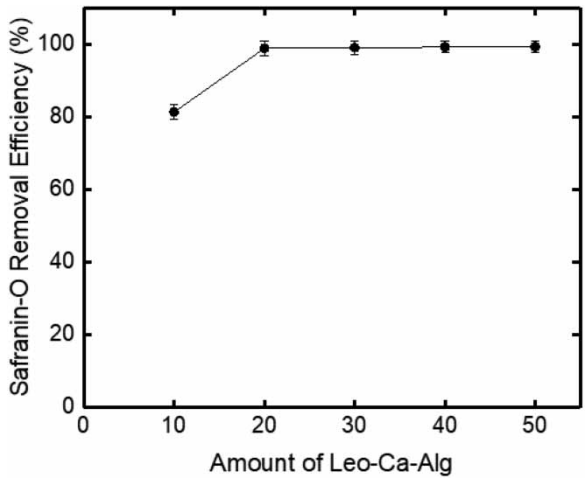

Figure 5 | The effect of Leo-Ca-Alg dose on the Safranin-O uptake efficiency (investigational circumstances: pH: 8; initial Safranin-O concentration: 10 mg/L; duration: 2 h; volume: 100 mL).

3.4. Contact time effects on the adsorption

Experiments were carried out to determine the effect of contact time on the adsorption process. Different solutions containing 10, 20, and 30 mg/L Safranin-O dye were prepared, and the pH was modified to 8. The optimum adsorbent dose (20 g/L) was added to each solution. Figure 6 shows the change in dye adsorption over 120 min for the different concentrations. The adsorption efficiencies gradually increased and exceeded 50% after the first 30 min. In the solution with a concentration of 10 mg/L dye, the value of 63.35% was observed rapidly within the first 15 min. Then, dye removal efficiencies and adsorption capacities continued to increase as the contact time with the adsorbent increased. At a concentration of 10 mg/L, 98.91% dye removal and 0.55 mg/g adsorption capacity were obtained in 120 min of contact time. The Safranin-O removal efficiency for the solutions with 20 and 30 mg/L concentrations reached 88.40 and 81.27%, respectively. While the uptake efficiency of the Safranin-O dye decreased with the concentration increases, the adsorption capacity increased to 0.88 and 1.22 mg/g for 20 and 30 mg/L solutions, respectively. The adsorption capacity improved at contact

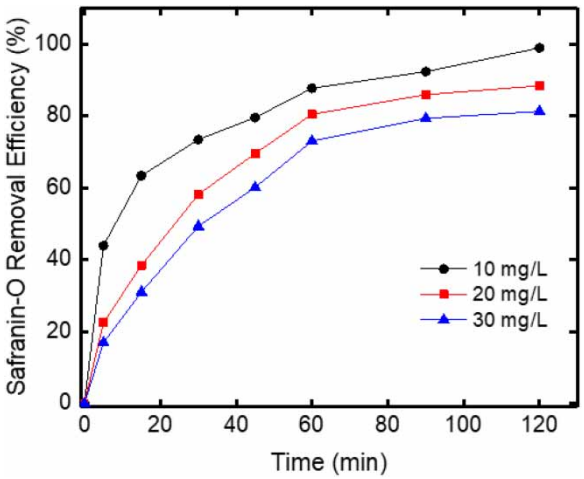

Figure 6 | The effect of contact time on the Safranin-O dye removal efficiency (investigational circumstances: adsorbent dose: 20 g/L; pH: 8; adsorption time: 2 h; volume: 100 mL).

time between 5 and 120 min. This indicates that during certain times, the active sites presented at the Leo-Ca-Alg were not filled optimally, and the adsorption equilibrium was not reached yet, and the adsorbent–adsorbate interaction was not occurred correctly (Mohamed *et al.* 2018). However, the values stabilized at a contact time of 120 min, which hinted that the adsorption equilibrium was realized. Thus, it may be reported that the optimal adsorption period was 120 min. Mohamed *et al.* (2018) found that in a solution containing 25 mg/L Safranin-O dye, the maximum adsorption capacity (13.76 mg/g) was attained at 240 min (Mohamed *et al.* 2018). Gun *et al.* (2022) noticed that the adsorption of Safranin-O dye onto the silica extracted from rice husk was very fast (Gun *et al.* 2022). In a previous study, the removal of 10, 25, and 50 mg/L cationic basic red 18 dye onto *Russula brevipes* after 5 min reached 78, 84, and 74%, respectively (Arslantaş *et al.* 2022).

3.5. Reuse stability of Leo-Ca-Alg beads

The reuse of Leo-Ca-Alg beads was evaluated at the optimum conditions (Safranin-O: 10 mg/L; Leo-Ca-Alg: 20 g/L; pH: 8; adsorption time: 120 min). At the end of the adsorption process, the adsorbent (Leo-Ca-Alg.) was collected. The collected beads were washed with a sufficient amount of distilled water (50 mL) and dried with paper. Subsequently, the beads were inserted again into dye solution and the adsorption process was accomplished again at the optimum conditions. The adsorption/desorption sequence was iterated 10 times. The removal efficiency for the first cycle was 98.91 and decreased to 94.43% dye removal efficiency after five cycles (Figure 7). For the sixth cycle, the removal efficiency was 89.82. Even in the 10th reuse, 83.01% removal efficiency was still achieved. The possibility of adsorbent losses during the adsorption/desorption cycles should be considered. These values showed that the recycling and reuse of the adsorbent are very high. The adsorbent material can be used repeatedly with no extra chemicals needed. The Leo-Ca-Alg beads have a recycling capability of 10 effective cycles, which is higher than the polyethyleneimine-Ca-Alg beads synthesized previously (Isik *et al.* 2021a).

3.6. Adsorption kinetics and isotherms

The kinetics study of the samples was carried out at different time intervals using pseudo-first-order, pseudo-second-order, and Elovich models. The pseudo-first-order model assumes that the dye removal is related to the diffusion force that depends on the differences in the solute concentrations. Also, the model interprets a linear proportion between the uptake and the difference in the saturation concentration, which is applicable just in the early steps of adsorption. In contrast, the pseudo-second-order kinetic model can predict the whole range of the adsorption process by the assumption of rate-liming steps as chemical sorption. For this model, the dominant factor affecting the adsorption rate is the adsorption capacity, not the dye concentration. The Elovich kinetic model utilizes the pseudo-second-order, supposing that the surface of the adsorbents is energetically heterogeneous (Lagergren 1898; Elovich & Larinov 1962; Ho *et al.* 1996; Saleh *et al.* 2022).

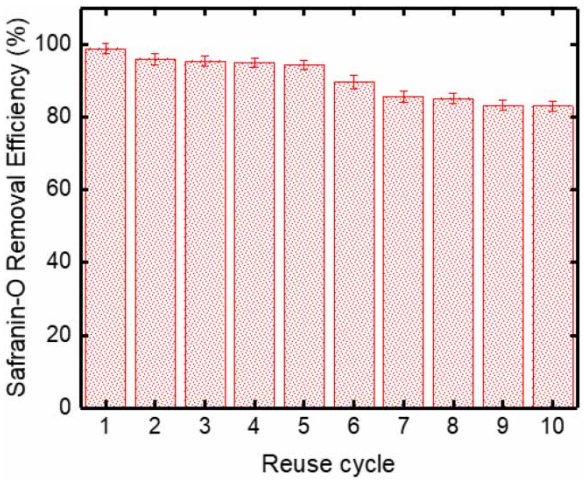

Figure 7 | Reuse number of adsorption/desorption experiments for Safranin-O uptake (investigational circumstances: dye concentration: 10 mg/L; adsorbent dose: 20 g/L; pH: 8; adsorption time: 120 min).

Table 2 presents the model-derived kinetic parameters and the statistical results. Accordingly, the three kinetic models had high correlation coefficients over the three concentrations. The adsorption at the lowest concentration (i.e. 10 mg/L) can be described by the Elovich model because it had the highest correlation coefficient and lowest chi-square error. However, the pseudo-second-order model described the adsorption at concentrations of 20 and 30 mg/L for the same reasons.

Table 2 | The kinetic parameters for the pseudo-first-order, pseudo-second-order, and Elovich models when Safranin-O was adsorbed onto Leo-Ca-Alg beads

Safranin-O	10 mg/L	20 mg/L	30 mg/L
First-order model			
$q_{e.}$(mg/g)	0.487 ± 0.021	0.885 ± 0.027	1.259 ± 0.037
k_1 (1/min)	0.094 ± 0.023	0.038 ± 0.004	0.031 ± 0.003
X^2 Red.	0.002	0.001	0.002
R^2	0.938	0.989	0.992
Second-order model			
q_e (mg/g)	0.548 ± 0.019	1.085 ± 0.040	1.606 ± 0.075
k_2 (g/mg min)	0.230 ± 0.048	0.038 ± 0.006	0.019 ± 0.003
X^2 Red.	5.97e-04	7.14e-04	0.002
$R^2_{\text{Adj.}}$	0.981	0.993	0.992
Elovich model			
a (mg/g·min)	0.220 ± 0.023	0.069 ± 0.011	0.066 ± 0.011
b (g/mg)	10.353 ± 0.291	3.722 ± 0.338	2.299 ± 0.250
X^2 Red.	4.07e-5	0.001	0.003
R^2 Adj.	0.998	0.989	0.987

The mechanism of the adsorption process of Safranin-O onto Leo-Ca-Alg beads was investigated using the IDM and Bangham models. According to Figure 8, the adsorption of Safranin-O onto Leo-Ca-Alg beads occurred in two steps. The first step referred to the ascending line, which indicated the adsorption speed at the adsorbent outer surface. The second step was a plateau, which included the movement of the particles to the pores.

Multi-linearity in the figure indicated that film diffusion contributed to adsorption. In addition, none of the lines crossed the origin point, indicating that pore diffusion alone does not contribute to rate control. The Bangham model results confirmed this mechanism (Table 3).

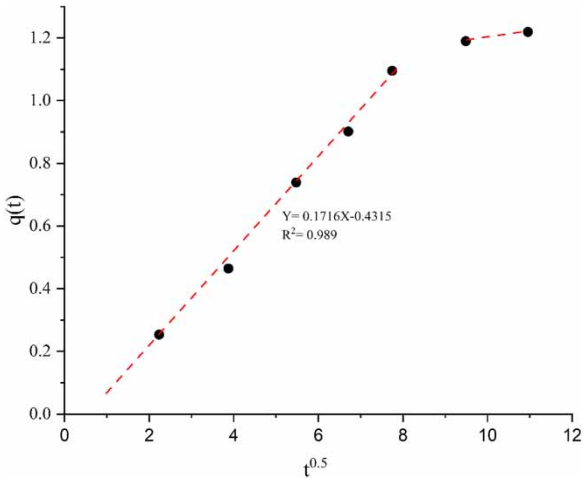

Figure 8 | IDM curve for the adsorption of Safranin-O onto the prepared Leo-Ca-Alg.

Table 3 | The Bangham model results for Safranin-O adsorption onto the prepared Leo-Ca-Alg

Safranin-O	10 ppm	20 ppm	30 ppm
K_b	1.146 ± 0.320	0.358 ± 0.050	0.266 ± 0.049
A	0.620 ± 0.095	0.737 ± 0.037	0.750 ± 0.047
X^2 Red.	6.86e-4	5.07e-4	0.002
R^2 Adj.	0.979	0.995	0.992

Adsorption isotherms relate adsorption capacity and adsorbate concentration at a constant temperature (Li *et al.* 2021). Because of liquid-phase adsorption complexity, there may not be a straightforward expression to illustrate the equilibrium adsorbent/adsorbate relationship. Therefore, Langmuir and Freundlich's models were used to describe the adsorption data. Table 4 shows the corresponding adsorption parameters derived from fitting data to the two isotherms. Based on the correlation coefficient values, the removal of Safranin-O dye by the Leo-Ca-Alg adsorbent can be defined by the Freundlich model. Accordingly, the adsorption ensues in a heterogeneous manner. Regarding the affinity factor value (n) emanated by the Freundlich isotherm, n located between 1 and 10 range isotherm revealed a high adsorbent adsorbate affinity (Tran *et al.* 2016).

Table 4 | Isotherm experiment results for the Safranin-O adsorption onto the prepared Leo-Ca-Alg beads

Isotherm	Parameter	Value
Langmuir	K_L (L/mg)	0.01809 ± 0.00635
	Q_{max} (mg/g)	3.43092 ± 0.84225
	X^2 Red.	0.00134
	R^2	0.98815
Freundlich	K_f ((mg/g) (L/mg)$^{1/n}$)	0.09787 ± 0.00977
	$1/n$	0.73995 ± 0.03129
	X^2 Red.	0.000319822
	R^2	0.99717

3.7. Adsorption thermodynamic

The thermodynamic parameters for the adsorption of Safranin-O onto the prepared Leo-Ca-Alg beads were specified at various temperatures (25, 30, and 35 °C). Table 5 shows the Gibbs free energy, enthalpy, and entropy.

The enthalpy change for the Safranin-O adsorption onto the prepared Leo-Ca-Alg beads was −176.60 kJ/mol. The adsorption can be typed as exothermic as the change in enthalpy was negative. The change in the entropy

Table 5 | Thermodynamic results for Safranin-O adsorption onto the prepared Leo-Ca-Alg

T (°C)	Δ*H* (kJ/mole)	Δ*S* (J/mole·K)	Δ*G*° (kJ/mole)
25	−176.5977	−562.2259	−9.054
30			−6.243
35			−3.432

reached −562.23 J/mole·K. The negative sign indicated that the Leo-Alg-Ca bead's surface randomness decreased at the end of the adsorption process (Dawood *et al.* 2016). Equations (10)–(12) are used in Gibbs's free energy calculation. Accordingly, ΔG° for Safranin-O adsorption at the temperatures of 298, 303, and 308 K were −9.05, −6.24, and −3.43 kJ/mole, respectively (Table 4). According to the negative sign of the Gibbs free energy change, the Safranin-O removal by Leo-Ca-Alg was feasible and naturally spontaneous (Biswas *et al.* 2020). Gibbs's free values were less than 20 kJ/mole, which indicated the physisorption type (Saleh *et al.* 2020). However, the kinetic experiments results showed a contribution of the chemisorption type in Safranin-O removal. Thus, the adsorption may be not relying on just one mechanism.

3.8. Comparison with other adsorbents

The prepared Leo-Ca-Alg beads were compared with other adsorbents. Table 6 shows a brief comparison with other adsorbents.

Table 6 | Comparison with other adsorbents

Adsorbent	Removal efficiency (%)	Kinetic	isotherm	Thermodynamic	Reusability	Reference
Leo-Ca-Alg	98.91	Elovich and pseudo-second-order model	Freundlich	Spontaneous and exothermic	10 cycles	This study
Magnetite/Ag nanocomposite	94	Particle diffusion-controlled mechanism	Langmuir	Spontaneous and endothermic	5 cycles	Salem *et al.* (2022)
Tea waste powder	93.7	–	Freundlich	Spontaneous and exothermic	–	Nehaba *et al.* (2019)
MgO decked multi-layered graphene	98	Pseudo-second-order model	Langmuir	–	3 cycles	Rotte *et al.* (2014)
Coconut coir	98	Pseudo-second-order model	Langmuir and Temkin	Spontaneous and exothermic	–	Ghosh *et al.* (2021)

4. CONCLUSION

In this study, it was examined the effect of leonardite powder embedded in Ca-Alg beads on Safranin-O removal. The effects of solution pH, Leo-Cal-Alg quantity, dye concentration, and temperature were explored. The reusability of the prepared adsorbent was investigated. In the adsorption process, it showed the best removal efficiency (98.91%) under pH 8, 20 g/L leonardite beads, 10 mg/L initial dye concentration, and temperature conditions at 25 °C. Low removal efficiency (2%) was obtained when bare Ca-Alg beads were tested for adsorption on the Safranin-O dye. When the effect of the initial dye concentration of Safranin-O was examined, it was observed that the removal efficiency decreased with the increased concentration. In reuse cycle studies, it was tried up to 10 reuses and decreased from 98.91 to 83.01% in the 10th use.

AUTHOR CONTRIBUTIONS

Nihan Canan Ozdemir helped in investigation and data curation. Mohammed Saleh helped in writing – original draft and formal analysis. Zeynep Bilici helped in methodology. Hudaverdi Arslan helped in review and editing.

Nadir Dizge helped in conceptualization, writing – original draft, and formal analysis. All authors commented on previous versions of the manuscript. All authors read and approved the final manuscript.

DATA AVAILABILITY STATEMENT

All relevant data are included in the paper or its Supplementary Information.

CONFLICT OF INTEREST

The authors declare there is no conflict.

REFERENCES

Abd-alla, M. A. & Aly, K. I. 1991 Arylidene polymers. IX. Synthesis, characterization, and morphology of new polyesters of diarylidenecycloalkanones containing thianthrene units. *Journal of Macromolecular Science – Chemistry* **28**, 251–267. https://doi.org/10.1080/00222339108052141.

Abou-Zeid, R. E., Ali, K. A., Gawad, R. M. A., Kamal, K. H., Kamel, S. & Khiari, R. 2021 Removal of Cu(II), Pb(II), Mg(II), and Fe(II) by adsorption onto alginate/nanocellulose beads as bio-sorbent. *Journal of Renewable Materials* **9**, 601–613. https://doi.org/10.32604/jrm.2021.014005.

Adegoke, K. A., Oyewole, R. O., Lasisi, B. M. & Bello, O. S. 2017 Abatement of organic pollutants using fly ash based adsorbents. *Water Science and Technology* **76**, 2580–2592. https://doi.org/10.2166/wst.2017.437.

Adel, M., Ahmed, M. A. & Mohamed, A. A. 2021 Synthesis and characterization of magnetically separable and recyclable crumbled $MgFe_2O_4$/reduced graphene oxide nanoparticles for removal of methylene blue dye from aqueous solutions. *Journal of Physics and Chemistry of Solids* **149**, 109760. https://doi.org/10.1016/j.jpcs.2020.109760.

Ahmad, M. A., Ahmad, N. & Bello, O. S. 2015 Modified durian seed as adsorbent for the removal of methyl red dye from aqueous solutions. *Applied Water Science* **5**, 407–423. https://doi.org/10.1007/s13201-014-0208-4.

Ahmad, M. A., Afandi, N. S., Adegoke, K. A. & Bello, O. S. 2016 Optimization and batch studies on adsorption of malachite green dye using rambutan seed activated carbon. *Desalination and Water Treatment* **57**, 21487–21511. https://doi.org/10.1080/19443994.2015.1119744.

Anbia, M., Hariri, S. A. & Ashrafizadeh, S. N. 2010 Adsorptive removal of anionic dyes by modified nanoporous silica SBA-3. *Applied Surface Science* **256**, 3228–3233. https://doi.org/10.1016/j.apsusc.2009.12.010.

Apostolidou, C., Sarris, E. & Georgakopoulos, A. 2022 Dynamic thermal aging of water-based drilling fluids with different types of low-rank coals as environmental friendly shear thinning additives. *Journal of Petroleum Science and Engineering* **208**, 109758. https://doi.org/10.1016/j.petrol.2021.109758.

Araujo, L. d., Borba, T. d., Ferreira, R. d. P., Canevesi, R. L. S., Silva, E. A. D., Dellamano, J. C. & Marumo, J. T. 2020 Use of calcium alginate beads and Saccharomyces cerevisiae for biosorption of 241am. *Journal of Environmental Radioactivity* **223–224**, 106399. https://doi.org/10.1016/j.jenvrad.2020.106399.

Arslantaş, C., M'barek, Saleh, M., Isik, Z., Ozdemir, S., Dundar, A. & Dizge, N. 2022 Leonardite powder as an efficient adsorbent for cationic and anionic dyes. *Water Environment Research* **94**, e10719. https://doi.org/10.1002/wer.10719.

Arslantaş, C., M'barek, I. & Saleh, M. *et al.* 2022 Basic Red 18 and Remazol Brilliant Blue R biosorption using *Russula brevipes*, *Agaricus augustus*, *Fomes fomentarius*. *Water Practice and Technology* **17**, 749–762. https://doi.org/10.2166/wpt.2022.008.

Bedade, D. K., Sutar, Y. B. & Singhal, R. S. 2019 Chitosan coated calcium alginate beads for covalent immobilization of acrylamidase: process parameters and removal of acrylamide from coffee. *Food Chemistry* **275**, 95–104. https://doi.org/10.1016/j.foodchem.2018.09.090.

Bensalah, J., Habsaoui, A., Dagdag, O., Lebkiri, A., Ismi, I., Rifi, E. H., Warad, I. & Zarrouk, A. 2021 Adsorption of a cationic dye (Safranin) by artificial cationic resins Amberlite®IRC-50: equilibrium, kinetic and thermodynamic study. *Chemical Data Collections* **35**, 100756. https://doi.org/10.1016/j.cdc.2021.100756.

Bilici, Z., Işık, Z., Aktaş, Y., Yatmaz, H. C. & Dizge, N. 2019 Photocatalytic effect of zinc oxide and magnetite entrapped calcium alginate beads for azo dye and hexavalent chromium removal from solutions. *Journal of Water Process Engineering* **31**, 100826. https://doi.org/10.1016/j.jwpe.2019.100826.

Biswas, S., Mohapatra, S. S., Kumari, U., Meikap, B. C. & Sen, T. K. 2020 Batch and continuous closed circuit semi-fluidized bed operation: removal of MB dye using sugarcane bagasse biochar and alginate composite adsorbents. *Journal of Environmental Chemical Engineering* **8**, 103637. https://doi.org/10.1016/j.jece.2019.103637.

Burakov, A. E., Galunin, E. V., Burakova, I. V., Kucherova, A. E., Agarwal, S., Tkachev, A. G. & Gupta, V. K. 2018 Adsorption of heavy metals on conventional and nanostructured materials for wastewater treatment purposes: a review. *Ecotoxicology and Environmental Safety* **148**, 702–712. https://doi.org/10.1016/j.ecoenv.2017.11.034.

Chammui, Y., Sooksamiti, P., Naksata, W., Thiansem, S. & Arqueropanyo, O. 2014 Removal of arsenic from aqueous solution by adsorption on leonardite. *Chemical Engineering Journal* **240**, 202–210. https://doi.org/10.1016/j.cej.2013.11.083.

Chanpiwat, P., Himeno, S. & Sthiannopkao, S. 2015 Arsenic and other metals' presence in biomarkers of Cambodians in arsenic contaminated areas. *IJERPH* **12**, 14285–14300. https://doi.org/10.3390/ijerph121114285.

Crini, G. 2006 Non-conventional low-cost adsorbents for dye removal: a review. *Bioresource Technology* **97**, 1061–1085. https://doi.org/10.1016/j.biortech.2005.05.001.

de Araújo, T. P., Quesada, H. B., dos Santos, D. F., Fonseca, B. C. D. S., Barbieri, J. Z., Bergamasco, R. & de Barros, M. A. S. D. 2022 Acetaminophen removal by calcium alginate/activated hydrochar composite beads: batch and fixed-bed studies. *International Journal of Biological Macromolecules* **203**, 553–562. https://doi.org/10.1016/j.ijbiomac.2022.01.177.

de Lima Barizão, A. C., Silva, M. F., Andrade, M., Brito, F. C., Gomes, R. G. & Bergamasco, R. 2020 Green synthesis of iron oxide nanoparticles for tartrazine and bordeaux red dye removal. *Journal of Environmental Chemical Engineering* **8**, 103618. https://doi.org/10.1016/j.jece.2019.103618.

Dawood, S., Sen, T. K. & Phan, C. 2016 Adsorption removal of Methylene Blue (MB) dye from aqueous solution by bio-char prepared from Eucalyptus sheathiana bark: kinetic, equilibrium, mechanism, thermodynamic and process design. *Desalination and Water Treatment* **57**:59, 28964–28980. https://doi.org/10.1080/19443994.2016.1188732.

Duman, O., Polat, T. G., Diker, C. Ö. & Tunç, S. 2020 Agar/κ-carrageenan composite hydrogel adsorbent for the removal of methylene blue from water. *International Journal of Biological Macromolecules* **160**, 823–835. https://doi.org/10.1016/j.ijbiomac.2020.05.191.

ElHussein, E. A. A., Şahin, S. & Bayazit, Ş. S. 2020 Removal of carbamazepine using UiO-66 and UiO-66/graphene nanoplatelet composite. *Journal of Environmental Chemical Engineering* **8**, 103898. https://doi.org/10.1016/j.jece.2020.103898.

Elovich, S. & Larinov, O. 1962 Theory of adsorption from solutions of non-electrolytes on solid (I) equation adsorption from solutions and the analysis of its simplest form,(II) verification of the equation of adsorption isotherm from solutions. *Izv AkadNauk SSSR, Otd Khim Nauk* **2**, 209–216.

Fiol, N., Poch, J. & Villaescusa, I. 2005 Grape stalks wastes encapsulated in calcium alginate beads for Cr(VI) removal from aqueous solutions. *Seperation Science and Technology* **40**, 1013–1028. https://doi.org/10.1081/SS-200048041.

Fourest, E. & Volesky, B. 1996 Contribution of sulfonate groups and alginate to heavy metal biosorption by the dry biomass of *Sargassum fluitans*. *Environmental Science & Technology* **30**, 277–282. https://doi.org/10.1021/es950315s.

Ghosh, I., Kar, S., Chatterjee, T., Bar, N. & Das, S. K. 2021 Adsorptive removal of Safranin-O dye from aqueous medium using coconut coir and its acid-treated forms: adsorption study, scale-up design, MPR and GA-ANN modeling. *Sustainable Chemistry and Pharmacy* **19**, 100374. https://doi.org/10.1016/j.scp.2021.100374.

Gok, C. & Aytas, S. 2009 Biosorption of uranium(VI) from aqueous solution using calcium alginate beads. *Journal of Hazardous Materials* **168**, 369–375. https://doi.org/10.1016/j.jhazmat.2009.02.063.

Gun, M., Arslan, H., Saleh, M., Yalvac, M. & Dizge, N. 2022 Optimization of silica extraction from rice husk using response surface methodology and adsorption of Safranin dye. *International Journal of Environmental Research* **16**, 20. https://doi.org/10.1007/s41742-022-00399-5.

Gupta, V. K., Mohan, D., Sharma, S. & Sharma, M. 2000 Removal of basic dyes (rhodamine b and methylene blue) from aqueous solutions using bagasse fly ash. *Separation Science and Technology* **35**(13), 2097–2113. http://doi.org/10.1081/SS-100102091.

Hanif, F., Ehsan, S., Zafar, S., Akhtar, M., Khan, M. I., Warsi, M. F., Mubarik, S., Hassan, W., Shakir, I. & Manzoor, S. 2020 Adsorptive removal of methyl orange and acid blue-2445 from binary system by anion exchange membrane BI: non-linear and linear form of isotherms. *DWT* **194**, 290–301. https://doi.org/10.5004/dwt.2020.25864.

Harris, R. G., Wells, J. D. & Johnson, B. B. 2001 Selective adsorption of dyes and other organic molecules to kaolinite and oxide surfaces. *Colloids and Surfaces A: Physicochemical and Engineering Aspects* **180**, 131–140.

Ho, Y., Wase, D. & Forster, C. 1996 Removal of lead ions from aqueous solution using sphagnum moss peat as adsorbent. *Water SA* **22**, 219–224.

Hu, S., Lin, X., Zhang, Y., Huang, R., Qu, Y., Luo, X. & Zhou, J. 2017 Preparation and application of alginate-Ca/attapulgite clay core/shell particle for the removal of uranium from aqueous solution. *Journal of Radioanalytical and Nuclear Chemistry* **314**, 307–319. https://doi.org/10.1007/s10967-017-5427-3.

Ip, A. W. M., Barford, J. P. & McKay, G. 2009 Reactive black dye adsorption/desorption onto different adsorbents: effect of salt, surface chemistry, pore size and surface area. *Journal of Colloid and Interface Science* **337**, 32–38. https://doi.org/10.1016/j.jcis.2009.05.015.

Isik, Z., Saleh, M., Bilici, Z. & Dizge, N. 2021a Remazol Brilliant Blue R (RBBR) dye and phosphate adsorption by calcium alginate beads modified with polyethyleneimine. *Water Environment Research* **93**, 2780–2794. https://doi.org/10.1002/wer.1635.

Isik, Z., Saleh, M. & Dizge, N. 2021b Adsorption studies of ammonia and phosphate ions onto calcium alginate beads. *Surfaces and Interfaces* **26**, 101330. https://doi.org/10.1016/j.surfin.2021.101330.

Kenawy, E.-R., Tenhu, H., Khattab, S. A., Eldeeb, A. A. & Azaam, M. M. 2022 Highly efficient adsorbent material for removal of methylene blue dye based on functionalized polyacrylonitrile. *European Polymer Journal* **169**, 111138. https://doi.org/10.1016/j.eurpolymj.2022.111138.

Khajavi, P., Keshtkar, A. R. & Moosavian, M. A. 2021 The optimization of U(VI) removal by a novel amidoximated modified calcium alginate gel bead with entrapped functionalized SiO2 nanoparticles. *Progress in Nuclear Energy* **140**, 103887. https://doi.org/10.1016/j.pnucene.2021.103887.

Lagergren, S. 1898 Zur theorie der sogenannten adsorption geloester stoffe, veternskapsakad. *Handlingar* **24**(4), 1–39.

Li, X., Qi, Y., Li, Y., Zhang, Y., He, X. & Wang, Y. 2013 Novel magnetic beads based on sodium alginate gel crosslinked by zirconium(IV) and their effective removal for Pb2+ in aqueous solutions by using a batch and continuous systems. *Bioresource Technology* **142**, 611–619. https://doi.org/10.1016/j.biortech.2013.05.081.

Li, W., Xie, Z., Xue, S., Ye, H., Liu, M., Shi, W. & Liu, Y. 2021 Studies on the adsorption of dyes, methylene blue, Safranin T, and malachite green onto polystyrene foam. *Separation and Purification Technology* **276**, 119435. https://doi.org/10.1016/j.seppur.2021.119435.

Liu, Q., Yu, H., Zeng, F., Li, X., Sun, J., Li, C., Lin, H. & Su, Z. 2021 HKUST-1 modified ultrastability cellulose/chitosan composite aerogel for highly efficient removal of methylene blue. *Carbohydrate Polymers* **255**, 117402. https://doi.org/10.1016/j.carbpol.2020.117402.

López-Luna, J., Ramírez-Montes, L. E. & Martinez-Vargas, S. *et al.* 2019 Linear and nonlinear kinetic and isotherm adsorption models for arsenic removal by manganese ferrite nanoparticles. *SN Applied Sciences* **1**, 950. https://doi.org/10.1007/s42452-019-0977-3.

Mallakpour, S. & Tabesh, F. 2019 Tragacanth gum based hydrogel nanocomposites for the adsorption of methylene blue: comparison of linear and non-linear forms of different adsorption isotherm and kinetics models. *International Journal of Biological Macromolecules* **133**, 754–766. https://doi.org/10.1016/j.ijbiomac.2019.04.129.

Mashkoor, F. & Nasar, A. 2020a Magnetized *Tectona grandis* sawdust as a novel adsorbent: preparation, characterization, and utilization for the removal of methylene blue from aqueous solution. *Cellulose* **27**, 2613–2635. https://doi.org/10.1007/s10570-019-02918-8.

Mashkoor, F. & Nasar, A. 2020b Magsorbents: potential candidates in wastewater treatment technology – a review on the removal of methylene blue dye. *Journal of Magnetism and Magnetic Materials* **500**, 166408. https://doi.org/10.1016/j.jmmm.2020.166408.

Maurya, N. S. & Mittal, A. K. 2013 Removal mechanism of cationic dye (Safranin O) from the aqueous phase by dead macro fungus biosorbent. *Water Science and Technology* **68**(5), 1048–1054. https://doi.org/10.2166/wst.2013.339.

Meng, F., Yuan, G. , Larson, S. L., Ballard, J. H., Waggoner, C. A., Arslan, Z., & Han, F. X. 2017 Removing uranium (VI) from aqueous solution with insoluble humic acid derived from leonardite. *Journal of Environmental Radioactivity* **180**, 1–8. https://doi.org/10.1016/j.jenvrad.2017.09.019.

Meng, F., Zhang, Y., Cai, Y., Yuan, G., & Han, F. X. 2021 Kinetic and thermodynamic features of Pb(II) removal from aqueous solution by leonardite-derived humic acid. *Water, Air, & Soil Pollution* **232**, 255. https://doi.org/10.1007/s11270-021-05223-y.

Mohamed, F., Abukhadra, M. R. & Shaban, M. 2018 Removal of safranin dye from water using polypyrrole nanofiber/Zn-Fe layered double hydroxide nanocomposite (Ppy NF/Zn-Fe LDH) of enhanced adsorption and photocatalytic properties. *Science of the Total Environment* **640–641**, 352–363. https://doi.org/10.1016/j.scitotenv.2018.05.316.

Mohan, D. & Chander, S. 2006 Removal and recovery of metal ions from acid mine drainage using lignite – a low cost sorbent. *Journal of Hazardous Materials* **137**, 1545–1553. https://doi.org/10.1016/j.jhazmat.2006.04.053.

Nehaba, S. S., Abdullah, R. H., Oda, A. M., Omran, A. R. & Mottaleb, A. S. 2019 Evaluation of the efficiency of tea waste powder to remove the Safranin O dye compared to the activated carbon as adsorbent. *Oriental Journal of Chemistry* **35**(3), 1201–1207. http://dx.doi.org/10.13005/ojc/350341.

Ngoc, P. K., Mac, T. K., Nguyen, H. T., Viet, D. T., Thanh, T. D., Vinh, P. V., Phan, B. T., Duong, A. T. & Das, R. 2022 Superior organic dye removal by CoCr2O4 nanoparticles: adsorption kinetics and isotherm. *Journal of Science: Advanced Materials and Devices* **7**, 100438. https://doi.org/10.1016/j.jsamd.2022.100438.

Ojo, T. A., Ojedokun, A. T. & Bello, O. S. 2019 Functionalization of powdered walnut shell with orthophosphoric acid for Congo red dye removal. *Particulate Science and Technology* **37**, 74–85. https://doi.org/10.1080/02726351.2017.1340914.

Ozuzun, S. & Uzal, B. 2021 Performance of leonardite humic acid as a novel superplasticizer in Portland cement systems. *Journal of Building Engineering* **42**, 103070. https://doi.org/10.1016/j.jobe.2021.103070.

Pham, T. D., Tran, T. T., Le, V. A., Pham, T. T., Dao, T. H. & Le, T. S. 2019 Adsorption characteristics of molecular oxytetracycline onto alumina particles: the role of surface modification with an anionic surfactant. *Journal of Molecular Liquids* **287**, 110900. https://doi.org/10.1016/j.molliq.2019.110900.

Ricca, G., Federico, L., Astori, C. & Gallo, R. 1993 Structural investigations of humic acid from leonardite by spectroscopic methods and thermal analysis. *Geoderma* **57**, 263–274. https://doi.org/10.1016/0016-7061(93)90009-A.

Rotte, N. K., Yerramala, S., Boniface, J. & Srikanth, V. V. S. S. 2014 Equilibrium and kinetics of Safranin O dye adsorption on MgO decked multi-layered graphene. *Chemical Engineering Journal* **258**, 412–419. https://doi.org/10.1016/j.cej.2014.07.065.

Roy, M., Saha, R., 2021 6 - Dyes and their removal technologies from wastewater: a critical review. In: *Intelligent Environmental Data Monitoring for Pollution Management* (Bhattacharyya, S., Mondal, N. K., Platos, J., Snášel, V., and Krömer, P., eds). Academic Press, pp. 127–160.

Sahu, M. K., Sahu, U. M. & Patel, R. K. 2015 Adsorption of safranin-O dye on CO_2 neutralized activated red mud waste: process modelling, analysis and optimization using statistical design. *RSC Advances* **5**(53), 42294–42304. https://doi.org/10.1039/C5RA03777H.

Saleh, M., Bilici, Z., Ozay, Y., Yabalak, E., Yalvac, M. & Dizge, N. 2020 Green synthesis of *Quercus coccifera* hydrochar in subcritical water medium and evaluation of its adsorption performance for BR18 dye. *Water Science and Technology* **83**, 701–714. https://doi.org/10.2166/wst.2020.607.

Saleh, M., Isik, Z., Yabalak, E., Yalvac, M. & Dizge, N. 2021 Green production of hydrochar nut group from waste materials in subcritical water medium and investigation of their adsorption performance for crystal violet. *Water Environment Research* **93**, 3075–3089. https://doi.org/10.1002/wer.1659.

Saleh, M., Isik, Z., Arslan, H., Yalvac, M. & Dizge, N. 2022 Adsorption of phosphate ions from aqueous solutions using marble, pumice, and basalt triple combination. *Water, Air, & Soil Pollution* **233**, 181. https://doi.org/10.1007/s11270-022-05637-2.

Salem, M. A., Salem, I. A., Zaki, H. M. & El-Sawy, A. M. 2022 Elimination of Safranin-O and a binary mixture of Safranin-O and methylene blue from water by adsorption on magnetite/Ag nanocomposite. *Egyptian Journal of Petroleum* **31**(2), 39–49. https://doi.org/10.1016/j.ejpe.2022.05.002.

Shi, W., Lü, C., He, J., En, H., Gao, M., Zhao, B., Zhou, B., Zhou, H., Liu, H. & Zhang, Y. 2018 Nature differences of humic acids fractions induced by extracted sequence as explanatory factors for binding characteristics of heavy metals. *Ecotoxicology and Environmental Safety* **154**, 59–68. https://doi.org/10.1016/j.ecoenv.2018.02.013.

Somsesta, N., Sricharoenchaikul, V. & Aht-Ong, D. 2020 Adsorption removal of methylene blue onto activated carbon/cellulose biocomposite films: equilibrium and kinetic studies. *Materials Chemistry and Physics* **240**, 122221. https://doi.org/10.1016/j.matchemphys.2019.122221.

Subba Reddy, Y., Maria Magdalane, C., Kaviyarasu, K., Mola, G. T., Kennedy, J. & Maaza, M. 2018 Equilibrium and kinetic studies of the adsorption of acid blue 9 and Safranin O from aqueous solutions by MgO decked FLG coated fuller's earth. *Journal of Physics and Chemistry of Solids* **123**, 43–51. https://doi.org/10.1016/j.jpcs.2018.07.009.

Tran, H. N., You, S.-J. & Chao, H.-P. 2016 Thermodynamic parameters of cadmium adsorption onto orange peel calculated from various methods: a comparison study. *Journal of Environmental Chemical Engineering* **4**, 2671–2682. https://doi.org/10.1016/j.jece.2016.05.009.

Yaneva, Z. L., Koumanova, B. K. & Georgieva, N. V. 2012 Linear and nonlinear regression methods for equilibrium modelling of p-nitrophenol biosorption by *Rhizopus oryzae*: comparison of error analysis criteria. *Journal of Chemistry* **2013**, 517631. https://doi.org/10.1155/2013/517631.

Yang, M., Xia, Y., Wang, Y., Zhao, X., Xue, Z., Quan, F., Geng, C. & Zhao, Z. 2016 Preparation and property investigation of crosslinked alginate/silicon dioxide nanocomposite films. *Journal of Applied Polymer Science* **133**. https://doi.org/10.1002/app.43489.

Zhou, Q., Wang, W., Liu, F. & Chen, R. 2022 Removal of difenoconazole and nitenpyram by composite calcium alginate beads during apple juice clarification. *Chemosphere* **286**, 131813. https://doi.org/10.1016/j.chemosphere.2021.131813.

First received 26 April 2023; accepted in revised form 18 June 2023. Available online 30 June 2023